Optical and Quantum Electronics (2024) 56:1200
https://doi.org/10.1007/s11082-024-07164-2

Design and analysis of all-optical reversible adder and subtractor using silicon microring resonator

V. Magesh[1] · J. Shirisha[2] · K. Lavanya[1] · Manjur Hossain[3]

Received: 27 March 2024 / Accepted: 4 June 2024

Abstract
Traditional logic circuit emits energy into the environment due to information loss, and it is referred to be irreversible logic circuits. Reversible logic circuit is capable of diminishing power loss, quantum cost, and garbage output. Many academics have recently embraced reversible logic-based circuits exploiting all-optical technology to conduct their research. In this article, all-optical reversible adder and subtractor have been implemented using microring resonator-based Naveen Raymond reversible logic gate, for the first time to our knowledge. MATLAB serves as the tool for design and analysis of the proposed architecture at almost 260 Gbps operational speed. The ultrafast response times and compact design of the microring resonator-based circuits make them especially useful for digital signal processing and communication systems. Some performance reflecting factors such as "quality factor", "photon cavity lifetime", "extinction ratio", "contrast ratio", "amplitude modulation", "on-off ratio", and "relative eye opening" are explored and analyzed. Optimized design parameters have been selected in order to build the model practically.

Keywords Microring resonator (MRR) · Adder · Subtractor · All-optical switch · Reversible logic gate

1 Introduction

In today's digital life, diminishing power dissipation is the serious goal of nanotechnology. Conventional logic circuits are irreversible, and the logic calculations involved in these circuits lose energy when information bits are lost. The energy wasted for losing a bit of data is kT*ln2 joules (Landauer 1961), where T is the absolute temperature of the procedure being conducted and k is the Boltzmann constant. Bennett (Bennett 1973) demonstrated that reversible logic (RL) for computation can result in zero energy

✉ Manjur Hossain
manjurhossain2003@gmail.com

[1] Velammal Engineering College, Chennai, Tamil Nadu 600066, India

[2] Malla Reddy Engineering College (Autonomous), Maisammaguda (H), Medchal-Malkajgiri District, Telangana 500100, India

[3] Department of Computer Science and Engineering, Saveetha School of Engineering, Saveetha Institute of Medical and Technical Sciences, Saveetha University, Chennai 602105, India

Published online: 18 June 2024

dissipation. Consequently, RL design has emerged as a feasible alternative to traditional logic design. The RL has a broad variety of applications in nanotechnology like optical computing and quantum computing, etc. (Fredkin 1990; Song et al. 2006). In RL circuit, each individual input produces an individual output and vice versa, resulting in a 1-to-1 mapping of input and output vectors. RL circuits exploit the lowest possible number of RL gates and unchanged inputs. RL also reduces both "garbage output (GO)" and "quantum cost (QC)". QC refers to the cost of every RL gate. RL has exclusive properties like no fan-out, no looping, etc. Also, the number of GOs, constant inputs and utilized gates will be reduced by employing RL. Fredkin, Toffoli (Fredkin and Toffoli 1982), Feynman (Feynman 1985), Peres gate (Peres 1985), are some example of useful RL gates.

The progress in recent digital signal processing and communication has encouraged experts to investigate data speeds approaching terabits per second. In order to achieve these speeds, the conventional carrier electron must be replaced by a photon. All-optical (AO) approaches have been used in a great deal of research and development in the field of photonics in recent years. This covers a broad range of mathematical and logical designs. Multiple AO approaches are "Mach Zehnder interferometer (MZI)", "semiconductor-optical amplifier (SOA)", "quantum-dot SOA (QD-SOA)", "terahertz-optical asymmetric de-multiplexers (TOAD)", "non-linear material (NLM)" and "microring resonator (MRR)", etc. (Qiu et al. 2020; Raja et al. 2021; Mukherjee 2021; Maji et al. 2023; Gosciniak et al. 2023; Singh et al. 2021; Hossain et al. 2022a; Kumar et al. 2021; Choure et al. 2023; Saharia et al. 2022) had been used to implement various arithmetical and logical designs for optical communication and signal processing. Two-photon absorption (TPA) can be used to accomplish all-optical switching in the context of tunable MRRs. A molecule or atom can absorb two photons at the same time by a nonlinear optical process called TPA, which produces an electronic transition with a larger energy than would be feasible with a single photon. As a result, TPA changes the refractive index of the material can lead to tunability in the resonance frequency of MRR. The nonlinear effects of TPA can be used to manipulate the amount of light that passes through the MRR by incorporating materials having TPA properties into these resonators. This phenomenon holds great significance for a number of applications, such as logic circuits and tunable MRRs. Also, the switching power of the TPA-based MRR switch is 3 orders smaller than that of the Kerr type MRR switch (Chun-Fei and Na 2009).

AO reversible adder and subtractor have been implemented by few researchers only. SOA-based MZI has been used to design reversible Naveen Raymond gate (NRG) to implement AO reversible adder and subtractor (Theresal et al. 2015). Another, SOA-based MZI has been implemented to design AO reversible adder and subtractor in Kotiyal et al. (2014). But, speed is limited for SOA-based devices (Kundu et al. 2023). For the first time to our knowledge, AO reversible NRG has been implemented using only MRRs to design reversible adder and subtractor which include the attractive characteristics of MRR, i.e. large "quality factor", "ultrafast switching", "compact size", "improved bandwidth", "low power consumption", "ease in fabrication", etc. (Soref 2006; Rakshit and Hossain 2022). MRR-based devices are ultra-fast because the "carrier lifetime" in an MRR cavity is very short, in the order of picoseconds (Xu and Lipson 2007).

The following is the order of proposed manuscript. Section 1 discusses about the reversible logic and the earlier works of AO reversible adder and subtractor. Section 2 illustrates the working of MRR-based AO switch. MRR-based reversible NRG, adder and subtractor have been discussed in Sect. 3. Section 4 covers the simulation results of MRR-based reversible NRG, adder and subtractor. Section 5 evaluates the important operational factors

that impact the efficiency of the proposed designs and the conclusion is mentioned in Sect. 6.

2 Silicon MRR: switching

MRR comprised of one (1) or two (2) straight waveguides (WGs) coupled to a circular-shaped WG which comes with four (4) ports represented in Fig. 1 (Rakshit and Hossain 2022). Input (I/P) is employed at the "add port (AP)" and "input port (IP)". The output (O/P) signal is identified at the "through port (TP)" and "drop port (DP)". A continuous wave (CW) optical probe signal is employed at the IP of MRR. The weak probe signal does not have any influence on the MRR material. The switching mechanism is come to realize by applying a strong optical signal from the top of the MRR. When the round-trip "optical path-length difference (OPD)" is an integer multiple of the MRR's resonant wavelength (λ_{res}), "ON resonance" of MRR occurs and only DP receives the signal that was employed at the IP. Free carriers are released in the MRR, after applying optical pump, due to "two-photon absorption (TPA)". The "refractive index (RI)" of the material is then changed via the "plasma-dispersion" effect (Xu and Lipson 2007). A π-phase shift will occur in the MRR and I/P signal is switched from DP to TP. Absence and presence of pump are identified by "logic 0" and "logic 1", respectively. Logically, DP and TP output can be expressed by '$\overline{A}$' and 'A', respectively if the pump is denoted by variable 'A'. O/P fields of DP and TP are expressed as below (Rakshit and Hossain 2022),

$$E_t = \frac{W\sqrt{1-k_1} - W\sqrt{1-k_2}x^2\exp^2(j\phi)}{1-\sqrt{1-k_1}\sqrt{1-k_2}x^2\exp^2(j\phi)}E_{i1} + \frac{-W\sqrt{k_1}\sqrt{k_2}x\exp(j\phi)}{1-\sqrt{1-k_1}\sqrt{1-k_2}x^2\exp^2(j\phi)}E_{i2} \tag{1}$$

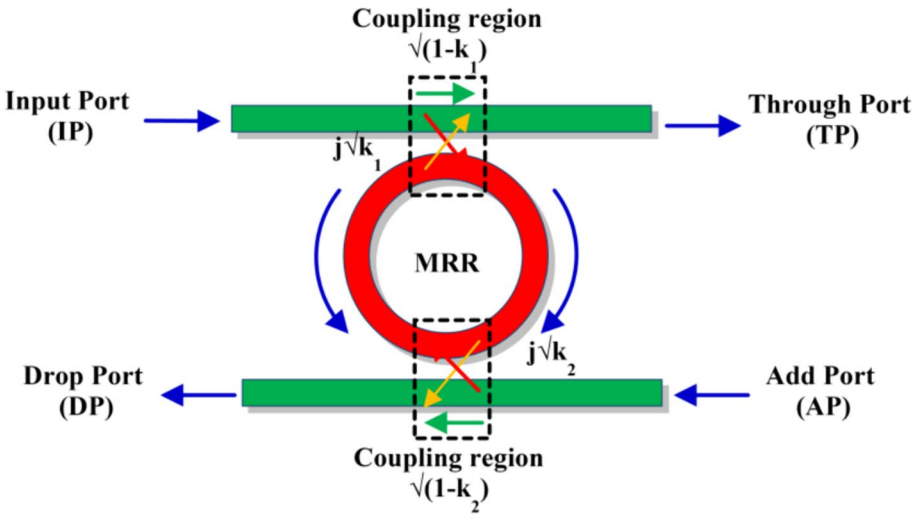

Fig. 1 MRR structure

$$E_d = \frac{-W\sqrt{k_1}\sqrt{k_2}x\exp(j\phi)}{1-\sqrt{1-k_1}\sqrt{1-k_2}x^2\exp^2(j\phi)}E_{i1} + \frac{W\sqrt{1-k_2}-G\sqrt{1-k_1}x^2\exp^2(j\phi)}{1-\sqrt{1-k_1}\sqrt{1-k_2}x^2\exp^2(j\phi)}E_{i2} \tag{2}$$

where $W=(1-\gamma)^{1/2}$, $x=W.\exp(-\frac{\alpha L}{4})$, $\phi=\frac{k_n.L}{2}$, k_1 (=0.22) is "coupling coefficient (CC)" between I/P WG and MRR, k_2 (=0.22) is CC between ring and O/P WG, "wave propagation constant" is k_n, where $k_n=\frac{2\pi}{\lambda}.n_{eff}$, "resonant wavelength" is λ_{res} (=1.55 μm), "intensity attenuation factor" (of MRR) is α (=0.0005 μm^{-1}) and "intensity insertion loss coefficient" of coupler is γ, ring length is L (=27.61 μm), E_{i1} is IP field and E_{i2} is AP field. The variations of DP and TP output intensity with respect to wavelength have been shown in Fig. 2.

Equations (1) and (2) look like static description but these equations are basically dynamic as Ei1 and Ei2 are time domain Gaussian laser source, though input Ei2 has not been used here. The below equation has been considered in MATLAB as the Gaussian optical pulse (Chun-Fei and Na 2009; Anashkina et al. 2016; Hong et al. 2017),

$$E_{i1}(t) = \frac{1}{\sigma\sqrt{2\pi}}e^{-\frac{1}{2}(\frac{t-\mu}{\sigma})^2}$$

where t is the time, μ = mean, σ = standard deviation. Other parameters of Eqs. (1) and (2) are optimized value.

Also, square signal can be applied to the MRR-based devices (Hossain et al. 2022a). At resonance, drop port output will remain high for a period of pulse width of respective Gaussian or square pulse.

Equation 3 and 4 convey a relationship between the phase shift and the RI of MRR when pump is applied (Hossain et al. 2022b),

$$Phase\ shift, \phi = \frac{2\pi}{\lambda}.\Delta nL \tag{3}$$

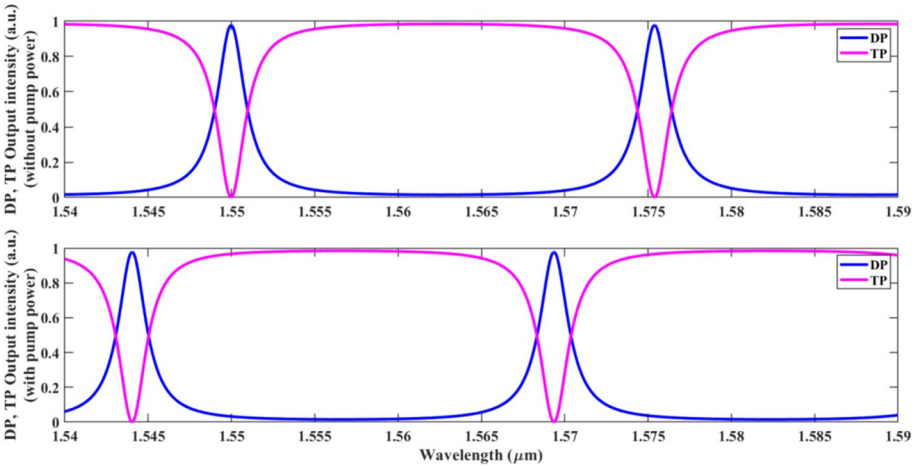

Fig. 2 Variation of DP, TP output intensity with respect to wavelength

$$\Delta n = -\left[8.8 \times 10^{-22} \frac{\beta t_p^2}{2h\upsilon\sqrt{\pi}\tau S^2} P_{av}^2 + 8.5 \times 10^{-22} \left(\frac{\beta t_p^2}{2h\upsilon\sqrt{\pi}\tau S^2} P_{av}^2\right)^{0.8}\right] \quad (4)$$

where P_{av} is "average pump power", t_p (=3.75 ps) is "pulse separation", τ (=200 fs) is the "pulse width", $h\upsilon$ (=49.725 × 10^{-20} J) is the "photon energy", and the "TPA coefficient" is β (=9.95 × 10^{-10} cm/W). A graph of phase change with average pump power is depicted in Fig. 3. A single MRR requires 1.01 mW of pump power to shift the I/P signal's phase to π.

3 MRR-based reversible adder and subtractor

Reversible adder and subtractor have been implemented using NRG. Again, MRR-based NRG requires XOR gate. For this design, MRR-based 2-input XOR and AND gate have been employed.

3.1 MRR-based all-optical XOR and AND gate

The XOR gate is a vital component for implementing AO reversible NRG. Its O/P will be "logic 0" if two I/Ps are "logic 0" or "logic 1", otherwise "logic 1". 2-I/P XOR gate using MRR has already been represented in our earlier work (Rakshit and Hossain 2022), which is shown in Fig. 4. The I/P signals are working as "pseudo-pump" signals for the MRR. Only one I/P is not enough to vary the "resonance" of the MRR. So, DP of MRR shows "logic 1" and TP of MRR shows "logic 0". If the two inputs are "logic 1", the total power of I/Ps are doubled and shift the resonance of MRR, DP shows "logic 0" and TP shows "logic 1" at this time. The operation of DP and TP verifies the 2-I/P XOR gate and AND gate, respectively which is represented in Table 1. Simulation of 2-I/P XOR and AND are given in Sect. 4.

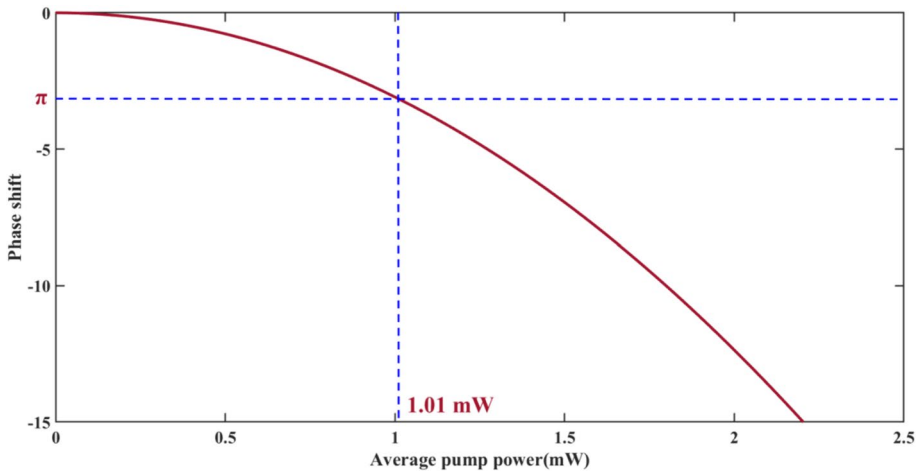

Fig. 3 Change in phase with regard to average pump power

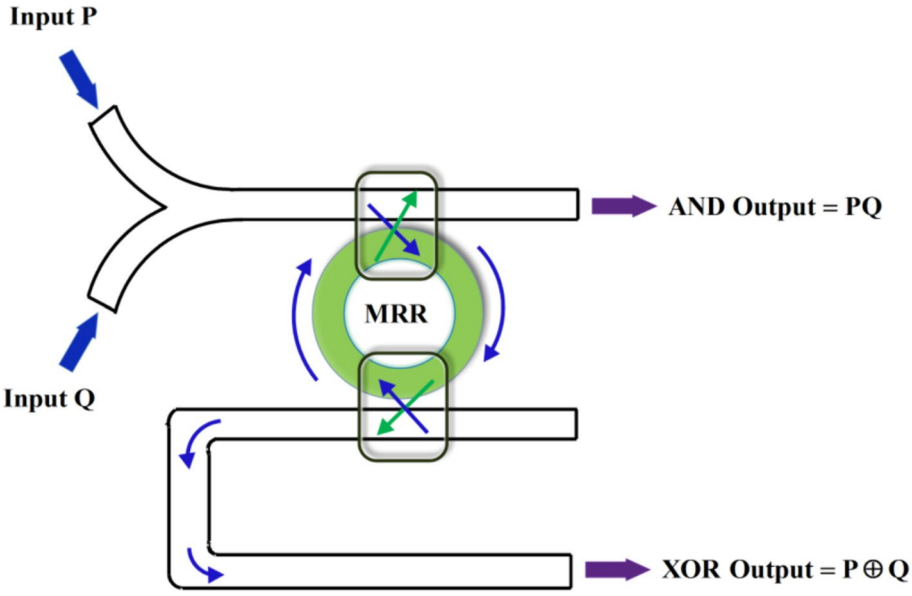

Fig. 4 MRR-based XOR and AND gate

Table 1 Truth table of XOR and AND gate

InputP	Input Q	Output at DP	Output at TP
0	0	0	0
0	1	1	0
1	0	1	0
1	1	0	1

3.2 MRR-based all-optical NRG

NRG is a 4×4 RL gate. The I/Ps are P, Q, R, S and the O/Ps be A, B, C, D respectively. NRG is employed to design reversible half adder (HA), half subtractor (HS), full adder (FA) and full subtractor (FS). One NRG unit is required to implement HA and HS, whereas two NRGs are required to implement FA and FS. The equations of NRG are expressed as follows (Theresal et al. 2015),

$$\left.\begin{aligned} A &= P \\ B &= P \oplus Q \\ C &= PQ \oplus R \\ D &= \overline{P}Q \oplus S \end{aligned}\right\} \tag{5}$$

The block representation of NRG is depicted in Fig. 5 and the corresponding truth table of NRG is given in Table 2.

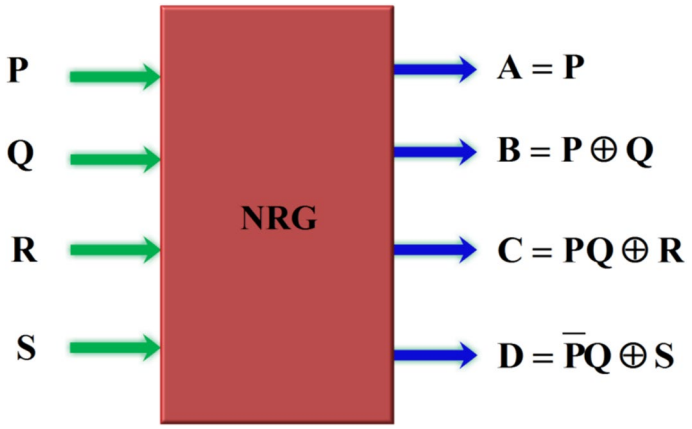

Fig. 5 Block representation of NRG

Table 2 Truth table of reversible NRG

I/Ps				O/Ps			
P	Q	R	S	A	B	C	D
0	0	0	0	0	0	0	0
0	0	0	1	0	0	0	1
0	0	1	0	0	0	1	0
0	0	1	1	0	0	1	1
0	1	0	0	0	1	0	1
0	1	0	1	0	1	0	0
0	1	1	0	0	1	1	1
0	1	1	1	0	1	1	0
1	0	0	0	1	1	0	0
1	0	0	1	1	1	0	1
1	0	1	0	1	1	1	0
1	0	1	1	1	1	1	1
1	1	0	0	1	0	1	0
1	1	0	1	1	0	1	1
1	1	1	0	1	0	0	0
1	1	1	1	1	0	0	1

In Table 2, P, Q, R and S are the inputs and A, B, C and D are the outputs. Output A from Table 2 can be expressed in sum of product (SOP) form,

$$\begin{aligned} A =& P.\overline{Q}.\overline{R}.\overline{S} + P.\overline{Q}.\overline{R}.S + P.\overline{Q}.R.\overline{S} + P.\overline{Q}.R.S \\ &+ P.Q.\overline{R}.\overline{S} + P.Q.\overline{R}.S + P.Q.R.\overline{S} + P.Q.R.S \\ =& P.\overline{Q}.\overline{R} + P.\overline{Q}.R + P.Q.\overline{R} + P.Q.R \\ =& P.\overline{Q} + P.Q = P \end{aligned}$$

Output B from Table 2 can be expressed in SOP form,

$$\begin{aligned}B =&\overline{P}.Q.\overline{R}.\overline{S} + \overline{P}.Q.\overline{R}.S + \overline{P}.Q.R.\overline{S} + \overline{P}.Q.R.\overline{S}\\ &+ P.\overline{Q}.\overline{R}.\overline{S} + P.\overline{Q}.\overline{R}.S + P.\overline{Q}.R.\overline{S} + P.\overline{Q}.R.S\\ =&\overline{P}.Q.\overline{R} + \overline{P}Q.R + P.\overline{Q}.\overline{R} + P.\overline{Q}.R\\ =&\overline{P}.Q + P.\overline{Q} = P \oplus Q\end{aligned}$$

Output C from Table 2 can be expressed in SOP form,

$$\begin{aligned}C =&\overline{P}.\overline{Q}.R.\overline{S} + \overline{P}.\overline{Q}.R.S + \overline{P}.Q.R.\overline{S} + \overline{P}.Q.R.S\\ &+ P.\overline{Q}.R.\overline{S} + P.\overline{Q}.R.S + P.Q.\overline{R}.\overline{S} + P.Q.\overline{R}.S\\ =&\overline{P}.\overline{Q}.R + \overline{P}.Q.R + P.\overline{Q}.R + P.Q.\overline{R}\\ =&\overline{P}.R + P.\overline{Q}.R + P.Q.\overline{R}\\ =&\mathrm{R}(\overline{P} + P.\overline{Q}) + P.Q.\overline{R}\\ =&\mathrm{R}(\overline{P} + \overline{Q}) + P.Q.\overline{R}\\ =&\overline{\mathrm{P.Q}}.\mathrm{R} + P.Q.\overline{R}\\ =&PQ \oplus \mathrm{R}\end{aligned}$$

Output D from Table 2 can be expressed in SOP form,

$$\begin{aligned}D =&\overline{PQ}.\overline{R}.S + \overline{P}.\overline{Q}.R.S + \overline{P}.Q.\overline{R}.\overline{S} + \overline{P}.Q.R.\overline{S}\\ &+ P.\overline{Q}.\overline{R}.S + P.\overline{Q}.R.S + P.Q.\overline{R}.S + P.Q.R.S\\ =&\overline{P}.\overline{Q}.S + \overline{P}.Q.\overline{S} + P.\overline{Q}.S + P.Q.S\\ =&\overline{PQ}.S + P.S + \overline{P}.Q.\overline{S}\\ =&\mathrm{S(P} + \overline{P}.\overline{Q}) + \overline{P}.Q.\overline{S}\\ =&\mathrm{S}(P + \overline{Q}) + \overline{P}.Q.\overline{S}\\ =&\mathrm{S}\overline{\overline{(P + \overline{Q})}} + \overline{P}Q.\overline{S}\\ =&\overline{(\overline{P}.Q)}S + \overline{P}.Q.\overline{S}\\ =&\overline{P}Q \oplus S\end{aligned}$$

Using these equations, Fig. 6 has been implemented.

NRG has been implemented using four MRRs, three beam splitters (BSs), five Erbium-doped waveguide amplifiers (EDWAs). The working of the proposed AO reversible NRG is given below that support the Eq. 5.

3.2.1 MRR1

Optical signal P and Q are applied to the MRR1. Optical signal P is split by BS1 and is applied to MRR1. Another part works as the output A. Optical signal Q is split by BS2 and is also applied to MRR1. Another part works as the pump signal for MRR3. The intensity of P is decreased due to BS1 and EDWA1 is used in the path so that it can be compensated by EDWA that uses the same WG material (i.e. silicon) (Bharti and Sonkar 2022; Agazzi et al. 2010). Similarly, the intensity of Q is decreased due to BS2 and EDWA2 and EDWA3

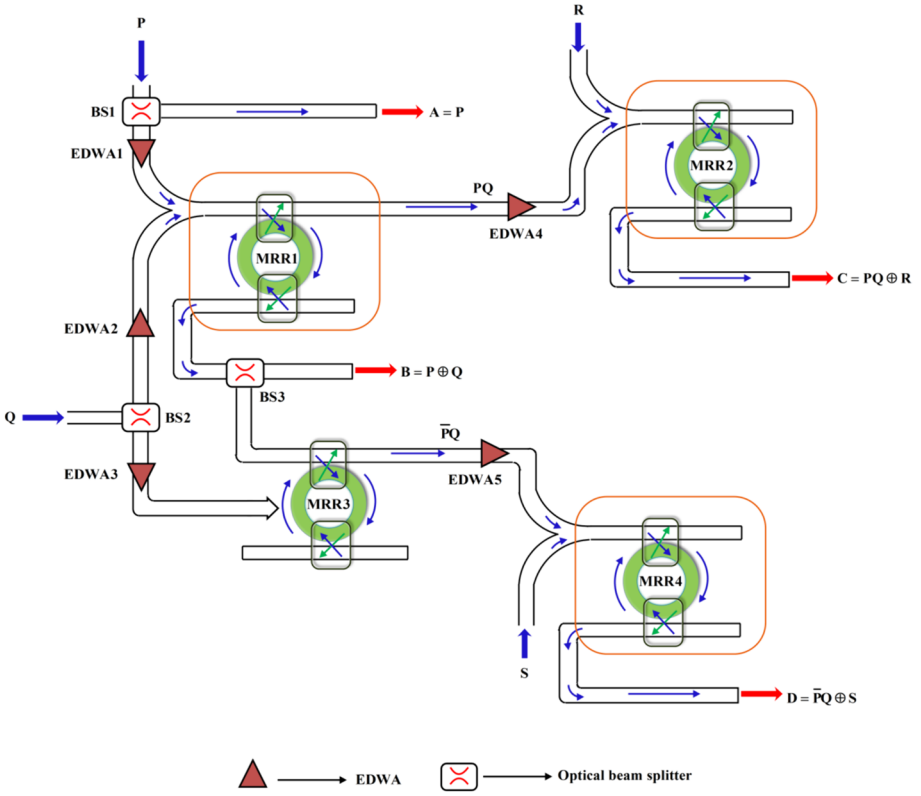

Fig. 6 MRR-based AO reversible NRG

are used in the path of MRR1 and MRR3 respectively. According to sub-Sect. 3.1, the DP and TP output of XOR1 will be $P \oplus Q$ and PQ respectively. The MRR and EDWA can be combined into a single module to keep the footprint small and the function completely manageable.

3.2.2 MRR2

Optical signal R and TP O/P of MRR1 (i.e. PQ) are applied to the MRR2. EDWA4 is used in the path of TP O/P of MRR1 so that it can be compensated. The DP output of XOR2 will be $PQ \oplus R$ i.e. output C.

3.2.3 MRR3

DP output is split by BS3 and is applied to the IP of MRR3. Another part works as the output B. Optical signal Q is split by BS2 and is also applied to MRR1. Another part works as the pump signal for MRR3 which is applied through EDWA3. According to MRR principle, the TP output of MRR3 will be Q $(P \oplus Q) = \overline{P}Q$.

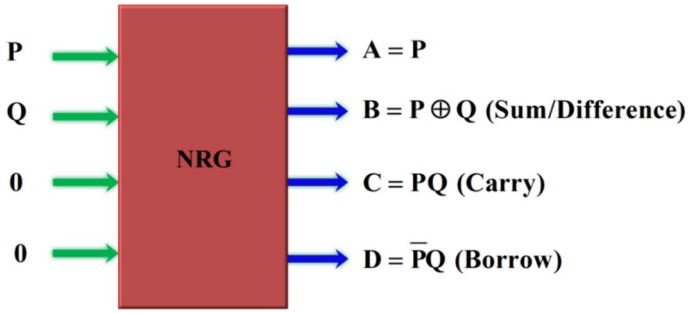

Fig. 7 Block representation of HA and HS using NRG

Table 3 Truth table of HA and HS

I/Ps		HA		HS	
		Sum	Carry	Difference	Borrow
P	Q	B	C	B	D
0	0	0	0	0	0
0	1	1	0	1	0
1	0	1	0	1	1
1	1	0	1	0	0

3.2.4 MRR4

Optical signal S and TP O/P of MRR3 (i.e. $\overline{P}Q$) are applied to the MRR4. TP O/P of MRR3 is applied through EDWA5. The DP output of MRR4 will be $\overline{P}Q \oplus S$ i.e. output D.

3.3 MRR-based all-optical reversible HA and HS using NRG

Reversible HA and HS are implanted using one NRG unit. Here, two I/Ps (R and S) are set to "logic 0" which are termed as "ancilla" input. The output B shows the sum or difference bit for HA and HS. The output C shows the carry bit for HA and the output D shows the borrow bit for HS. The block diagram for HA and HS using NRG is shown in Fig. 7 and the truth table for the HA and HS are shown in Table 3.

3.4 MRR-based all-optical reversible FA and FS using NRG

Reversible FA and FS are implanted using two NRG units (NRG1 and NRG2). Here, two I/P bits P and Q are applied to NRG1. The O/Ps of NRG1 ($P \oplus Q$, PQ and $\overline{P}Q$) and input carry or borrow bit (R) are connected to NRG2 as shown in Fig. 8. The sum and output carry bit for FA are realized from the output B and C of NRG2 respectively. The difference and output borrow bit for FS are realized from the output B and D of NRG2 respectively. The truth table for the FA and FS are shown in Tables 4 and 5 respectively. The equations for output carry and borrow have been verified with the standard equations for FA and FS.

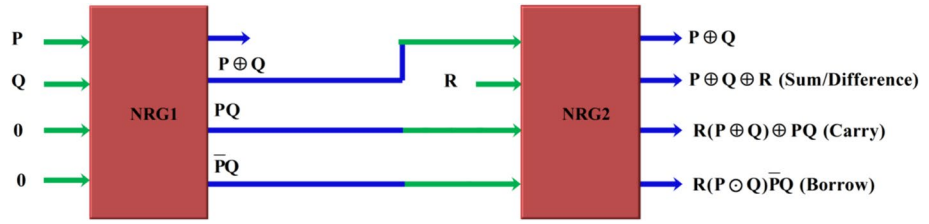

Fig. 8 Block representation of FA and FS using NRG

Table 4 Truth table of FA

Inputs			Outputs	
P	Q	Input carry, R	Sum	Output carry
0	0	0	0	0
0	0	1	1	0
0	1	0	1	0
0	1	1	0	1
1	0	0	1	0
1	0	1	0	1
1	1	0	0	1
1	1	1	1	1

Table 5 Truth table of FS

Inputs			Outputs	
P	Q	Input borrow, R	Sum	Output borrow
0	0	0	0	0
0	0	1	1	1
0	1	0	1	1
0	1	1	0	1
1	0	0	1	0
1	0	1	0	0
1	1	0	0	0
1	1	1	1	1

4 Simulation results

For simulation purpose, "MATLAB" program is used. The optimum settings are similar to those in Hossain et al. 2022b, excluding the MRR radius (4.395 μm). For pump signal, "logic 0" means its absence, whereas "logic 1" means its presence. For data pulse, "logic 0" and "logic 1" are declared by absence and presence of optical signal with 0.505 mW, respectively. MATLAB simulation of 2-input XOR and AND gate is depicted in Fig. 9. The simulation of NRG is presented in Fig. 10. The simulation of HA

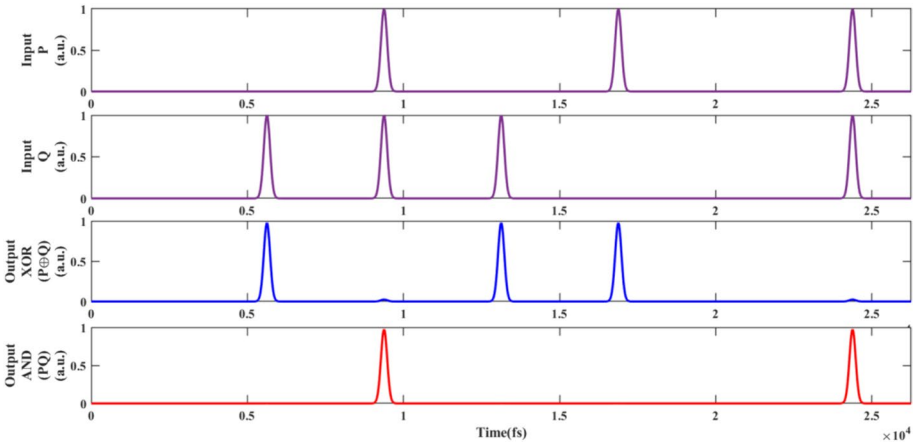

Fig. 9 MATLAB simulation of 2-input XOR and AND gate

and HS is shown in Fig. 11. The same for FA and FS are depicted in Fig. 12 and Fig. 13 respectively.

5 Discussion

The "pulse width" and "pulse period" of the data pulse used in the circuit being proposed, have an effect on the speed of the device. The modeled circuit uses "picosecond mode-locked fibre laser" as a data pulse. Its "pulse duration" is 3.75 ps (Deslandes et al. 2013). The switching time from drop port to through port or vice-versa is 3.75 ps. It can be basically thought of as time delay of the MRR. So, the evaluated "switching speed" of the circuit is (1/3.75) ps, which is nearly 260 Gbps. By utilizing variable femtosecond lasers, data rate can be adjusted (Sibbett et al. 2012).

Moreover, operational speed is also dependent on the "free carrier (photon) lifetime" in MRR. To avoid "inter-symbol interference", the free carriers created by the applied optical pulse in the MRR should be recombined before the arrival of subsequent pulse. The "carrier lifetime $\left(\tau_{\text{cav}}\right)$" is defined as (Xu and Lipson 2007),

$$\tau_{\text{cav}} = Q\lambda_{res}/(2\pi c) \tag{6}$$

where c is the "speed of light" (in vacuum), Q is "quality factor" of MRR. The "full width at half maximum (FWHM)" and λ_{res} values are used to find the Q. The FWHM and λ_{res} values for the circuit we have proposed are 2 nm and 1550 nm, respectively. The value of Q is 775. The value of τ_{cav} is 0.64 ps, which is smaller than the "pulse duration" of 3.75 ps.

Any design that wishes to be evaluated for efficiency must have its performance metrics examined. "Extinction ratio (ER)", "contrast ratio (CR)", "amplitude modulation (AM)", "on–off ratio (OOR)" and "pseudo eye diagram (PED)" are obtained numerically from "MATLAB" simulation of NRG. These parameters show the excellence of O/P signal. To eliminate noise, strengthen SNR, and make resonance simpler to detect, AM should be smaller while CR and ER should have higher value. A CR and ER level of 10 dB is adequate to guarantee that the majority of I/P is directed towards the O/P (Chao and Guo 2006). However, the AM level must be less than one decibel (Vardakas and Zoiros 2007).

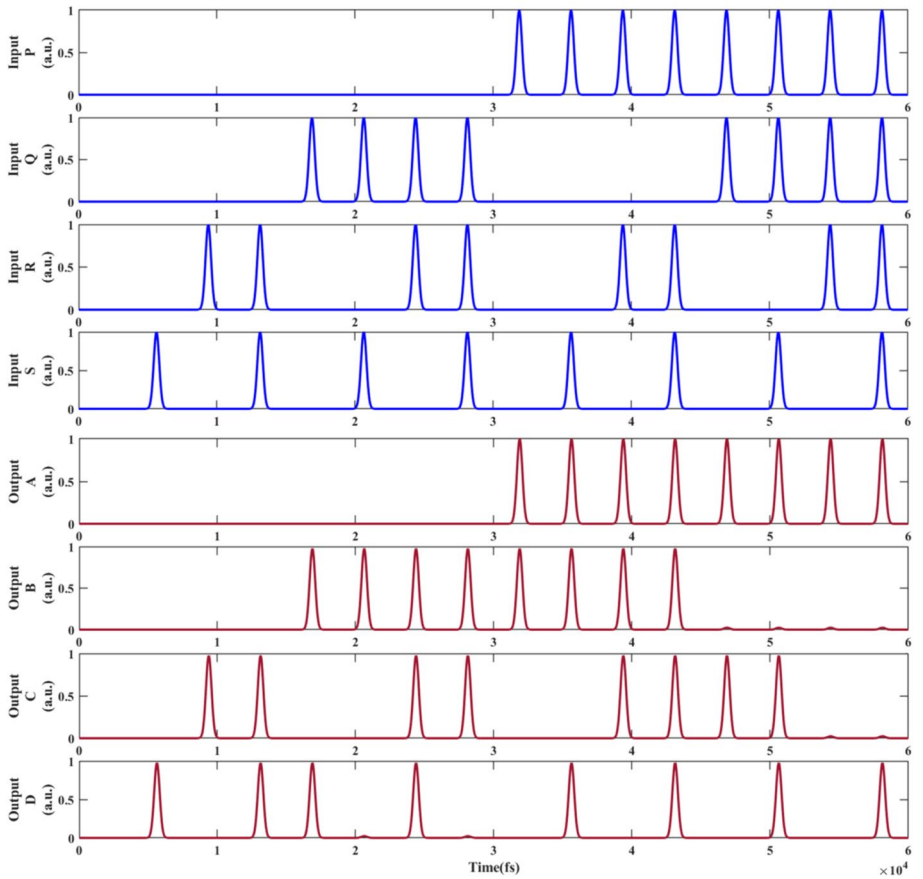

Fig. 10 MATLAB simulation of NRG

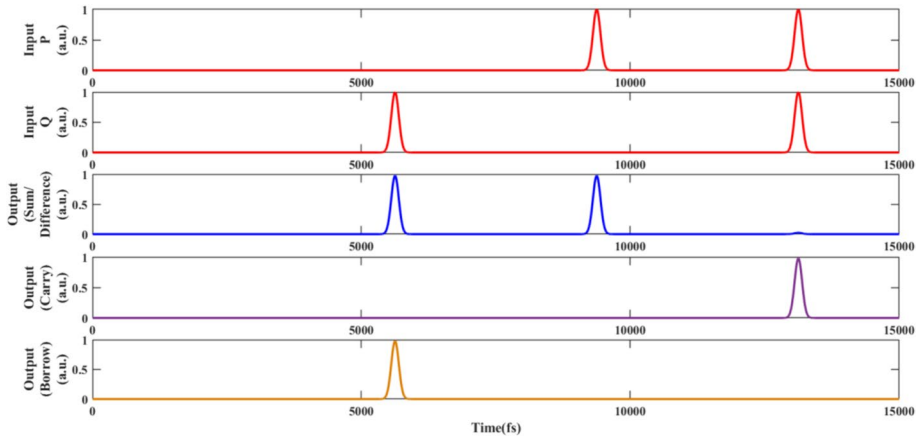

Fig. 11 MATLAB simulation of HA and HS

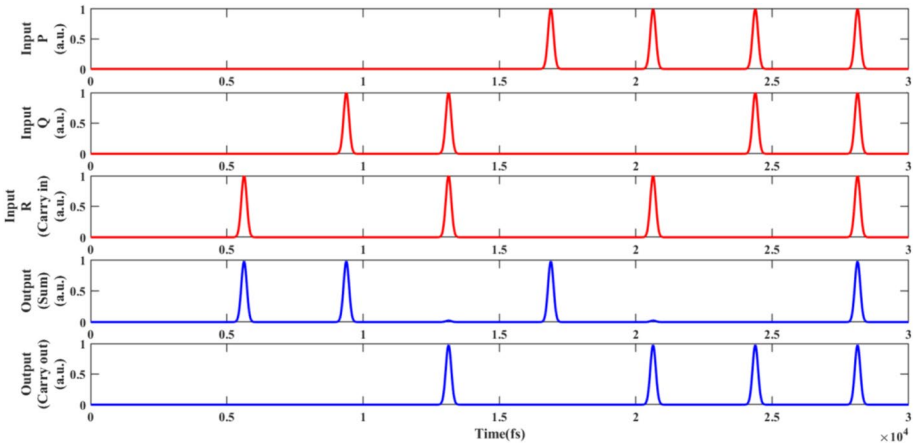

Fig. 12 MATLAB simulation of FA

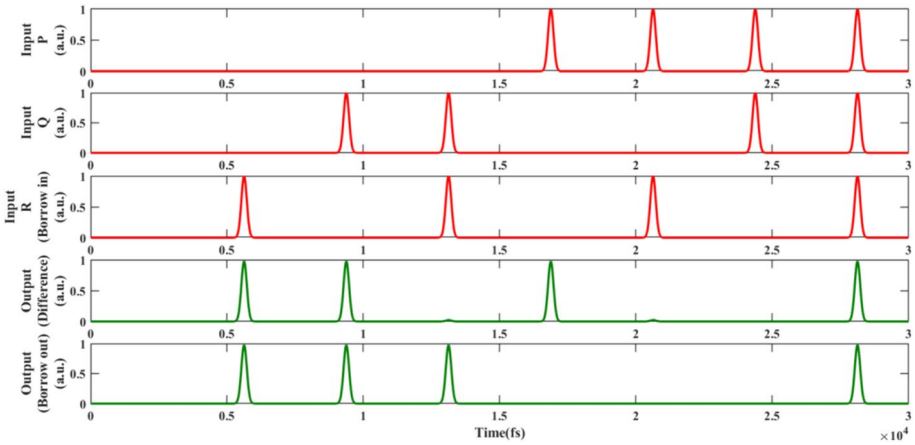

Fig. 13 MATLAB simulation of FS

The ER is explained in dB as (Hossain et al. 2023a),

$$\mathrm{ER(dB)} = 10\log\left(\frac{P^{1}_{\min}}{P^{0}_{\max}}\right) \tag{7}$$

where $P^{1}_{\min}$ is "minimum" peak intensity for "logic 1" and $P^{0}_{\max}$ is "maximum" peak intensity for "logic 0". ER versus CCs is depicted with unchanged radius (4.395 μm) in Fig. 14a. Similarly, ER versus MRR radii is depicted with the unchanged CC (0.22) in Fig. 14b. ER of the device is 15.96 dB with optimized parameters.

The ratio of mean or average O/P for "logic 1" (P^{1}_{mean}) and mean or average O/P for "logic 0" (P^{0}_{mean}) is referred to CR, and showed in decibel (Hossain et al. 2023a),

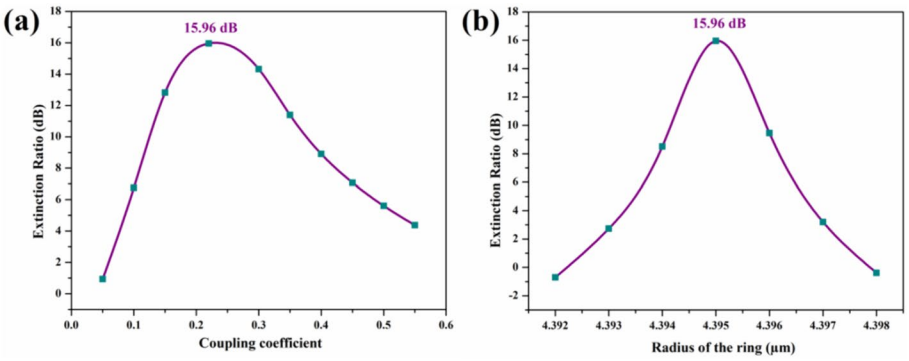

Fig. 14 ER versus **a** CCs **b** ring radii

$$\text{CR (dB)} = 10\log\left(\frac{P^1_{mean}}{P^0_{mean}}\right) \tag{8}$$

Figure 15a represents the graph of CR versus CCs with fixed radius (4.395 μm) and Fig. 15b represents the graph of CR versus MRR radii with fixed CC (0.22). CR of the device being implemented is 22.37 dB with optimized values.

The AM is measures in decibels as (Hossain et al. 2023b),

$$\text{AM (dB)} = 10\log\left(\frac{P^1_{\max}}{P^1_{\min}}\right) \tag{9}$$

where, $P^1_{\max}$ is "maximum" O/P values for "logic 1". Figure 16a demonstrates AM versus CCs with constant radius (4.395 μm). AM versus MRR radii with unchanged CC (0.22) is demonstrated in Fig. 6b. AM is 0.013 dB at optimal values.

Synchronization of narrow pulses is difficult if different sources are used. Synchronization problem can be minimized by using single source. Inverted input can be generated by an inverter circuit controlled to source. This type of source is also applied in Sethi and Roy (2013).

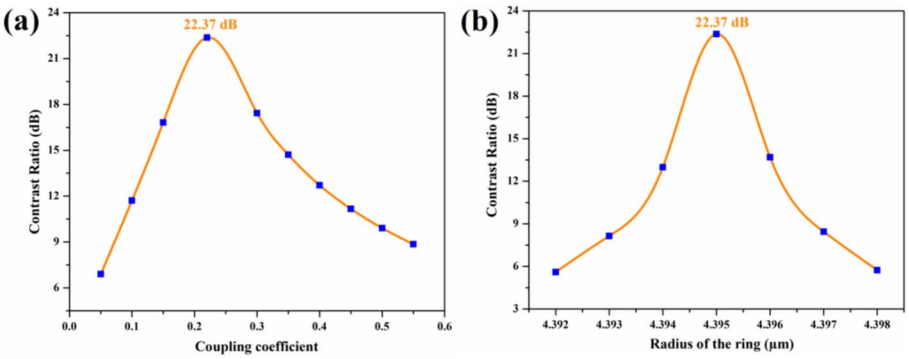

Fig. 15 CR versus **a** CC **b** ring radii

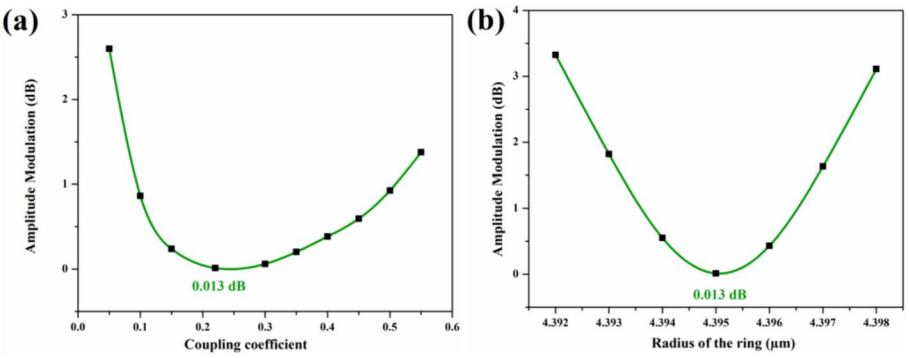

Fig. 16 AM versus **a** CC **b** ring radii

However, if the inputs are not synchronized, the minimum and maximum level of logic '1' and logic '0' can be of any value. Hence, the value of ER, CR and relative eye opening will be decreased and value of AM will be increased. So, the output will be distorted and affect the performance of the device.

Equations 7–9 are used to find the value of ER, CR and AM. Also, Fig. 10 has been used to extract the data for ER, CR and AM. Here, MRR3 of Fig. 6 is only considered to vary the coupling co-efficient or MRR radius. At one instance, MRR3 radius is fixed and coupling co-efficient is changing gradually. At second instant, coupling co-efficient is fixed and MRR radius is changing gradually. So, the maximum and minimum intensity for logic '1' and logic '0' will be varied which can be observed from Fig. 10.

The OOR is evaluated by ratio of DP (T_{max}) and TP (T_{min}) intensity at resonance (Hossain et al. 2023b),

$$OOR = \frac{T_{\max(Drop\,port)}}{T_{\min(Through\,port)}} \tag{10}$$

For the system to work efficiently, the OOR must be greater than 20 decibels. Figure 17 depicts the OOR, which is 39.11 dB.

An additional parameter is the pseudo eye diagram (PED) (Hong et al. 2017; Chao and Guo 2006; Freude et al. 2012; https://optics.ansys.com/hc/en-us/articles/360036107074-Eye-Diagram-EYE-NTERCONNECT-Element). It is evident that the envelopes of the 1-states and the 0-states can be easily differentiated from one another. The envelopes of the logic spaces have been strongly repressed, whereas the envelopes of marks have a manageable vertical separation between them (Vardakas and Zoiros 2007). The PED for NRG is given in Fig. 18a. The PED for HA and HS is given in Fig. 18b. The PED for FA and FS is given in Fig. 18c. PED is depicted by the overlapping of every potential O/P. The "logic 0" and "logic 1" envelopes may sharply be distinctive. The "relative eye opening (O)" is a supplementary factor of PED quality (Hossain et al. 2023b),

$$O = \frac{(P^1_{\min} - P^0_{\max})}{P^1_{\min}} \tag{11}$$

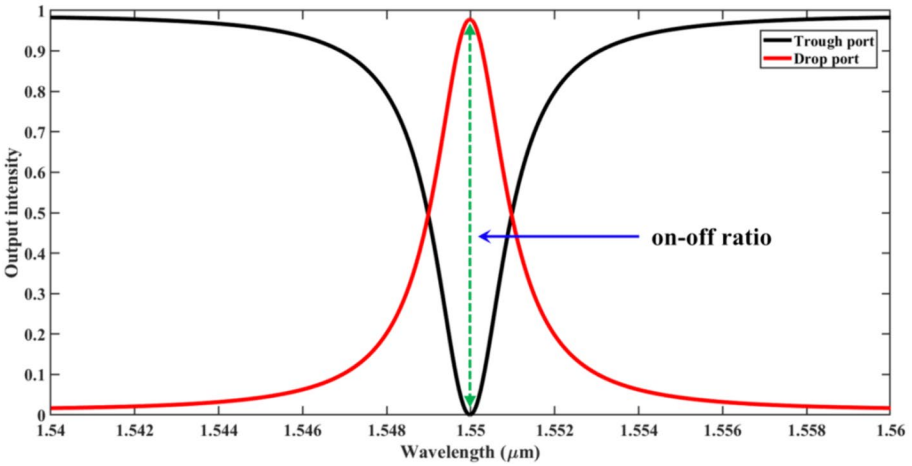

Fig. 17 On–off ratio

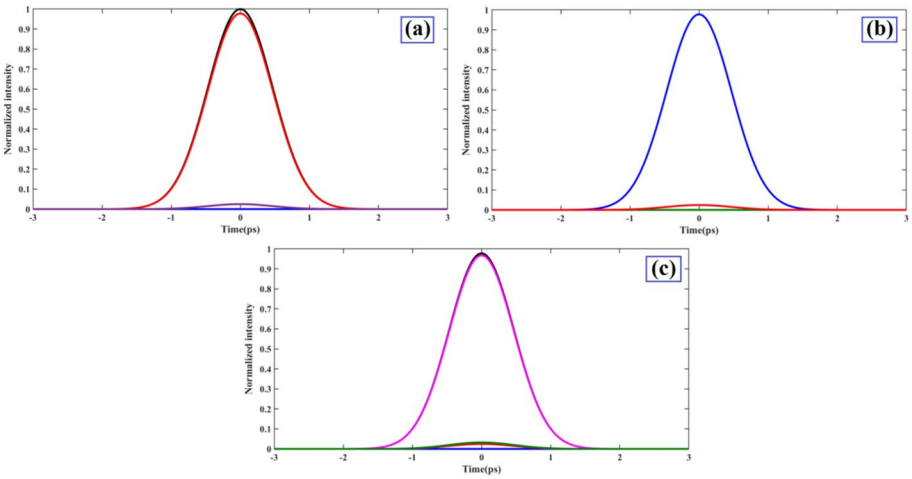

Fig. 18 PED of AO reversible **a** NRG **b** HA and HS **c** FA and FS

$O = 97.40\%$ for reversible NRG, $O = 97.40\%$ for reversible HA and HS. $O = 96.80\%$ for reversible FA and FS.

6 Conclusion

In conclusion, MRR-based all-optical reversible adder and subtractor have been designed exploiting MRR-based Naveen Raymond reversible logic gate. Naveen Raymond reversible logic gate has been implemented using four MRRs only. All the proposed designs have been numerically analyzed and verified against the truth table using MATLAB software. An MRR requires only 1.01 mW of pump power to cause the switching phenomenon.

Furthermore, the proposed circuits can work at a speed of nearly 260 Gbps. CR and ER has their respective values of 22.37 dB and 15.96 dB. AM is 0.013 dB. The value of "on–off ratio" is 39.11 dB at optimized parameter. The achieved Q factor is 775. The relative eye opening is 97.40% for reversible NRG, half adder and half subtractor, and 96.80% for full adder and full subtractor.

Author contributions Magesh V—Methodology, implementation, simulation and writing original draft preparation. Shirisha J—Simulation, reviewing and editing the draft manuscript. Lavanya K—Implementation, Reviewing and editing the draft manuscript. Manjur Hossain—Conceptualization, supervision, reviewing and editing the draft manuscript.

Funding There was no funding for this research project.

Availability of data and materials Not applicable.

Code availability Not applicable.

Declarations

Conflict of interest The authors have declared no conflict of interest.

Ethical approval This article does not contain any studies with human participants or animals performed by any of the authors.

Consent to participate All authors are agreed and gave their consent to participate in this research work.

Consent for publication All authors are agreed and gave their consent for the publication of this research paper.

References

Agazzi, L., Bradley, J.D., Dijkstra, M., Ay, F., Roelkens, G., Baets, R., Wörhoff, K., Pollnau, M.: Monolithic integration of erbium-doped amplifiers with silicon-on-insulator waveguides. Opt. Express **18**(26), 27703–27711 (2010)

Anashkina, E.A., Ginzburg, V.N., Kochetkov, A.A., Yakovlev, I.V., Kim, A.V., Khazanov, E.A.: Single-shot laser pulse reconstruction based on self-phase modulated spectra measurements. Sci. Rep. **6**(1), 33749 (2016)

Bennett, C.H.: Logical reversibility of computation. IBM J. Res. Dev. **17**(6), 525–532 (1973)

Bharti, G.K., Sonkar, R.K.: Design and performance analysis of all-optical D and T flip-flop in a polarization rotation based micro-ring resonator. Opt. Quant. Electron. **54**(3), 176 (2022)

Chao, C.Y., Guo, L.J.: Design and optimization of microring resonators in biochemical sensing applications. J. Lightwave Technol. **24**(3), 1395–1402 (2006)

Choure, K.K., Saharia, A., Mudgal, N., Pandey, R., Agarwal, A., Prajapat, M., Maddila, R., Tiwari, M., Singh, G.: Reconfigurable and compact reversible channel multiplexers using Si3N4 based optical microring resonator. Optics Communications **530**, 129126 (2023)

Chun-Fei, L., Na, D.: Optical switching in silicon nanowaveguide ring resonators based on Kerr effect and TPA effect. Chin. Phys. Lett. **26**(5), 054203 (2009)

Deslandes, P., Perrin, M., Saby, J., Sangla, D., Salin, F., Freysz, E.: Picosecond to femtosecond pulses from high power self mode–locked ytterbium rod-type fiber laser. Opt. Express **21**(9), 10731–10738 (2013)

Feynman, R.P.: Quantum mechanical computers. Optics News **11**(2), 11–20 (1985)

Fredkin, E.: An informational process based on reversible universal cellular automata. Physica D **45**(1–3), 254–270 (1990)

Fredkin, E., Toffoli, T.: Conservative logic. Int. J. Theor. Phys. **21**(3), 219–253 (1982)

Freude, W., Schmogrow, R., Nebendahl, B., Winter, M., Josten, A., Hillerkuss, D., Koenig, S., Meyer, J., Dreschmann, M., Huebner, M., Koos, C.: Quality metrics for optical signals: Eye diagram, Q-factor, OSNR, EVM and BER. In 2012 14th Int. Conference on Transparent Optical Networks (ICTON), IEEE. 1–4 (2012)

Gosciniak, J., Hu, Z., Thomaschewski, M., Sorger, V.J., Khurgin, J.B.: Bistable All-Optical Devices Based on Nonlinear Epsilon-Near-Zero (ENZ) Materials. Laser Photonics Rev. **17**(4), 2200723 (2023)
Hong, J., Qiu, F., Cheng, X., Spring, A.M., Yokoyama, S.: A high-speed electro-optic triple-microring resonator modulator. Sci. Rep. **7**(1), 4682 (2017)
Hossain, M., Rakshit, J.K., Zoiros, K.E.: Microring resonator-based all-optical parallel pseudo random binary sequence generator for rate multiplication. Opt. Quant. Electron. **54**(8), 525 (2022a)
Hossain, M., Rakshit, J.K., Chattopadhyay, T.: Silicon microring resonator based on all-optical reversible modified Fredkin gate: design and analysis. Opt. Eng. **61**(4), 046111–046111 (2022b)
Hossain, M., Rakshit, J.K., Bhatnagar, A., Chattopadhyay, T.: Silicon microring resonator based all-optical 3-input majority gate and its applications. Optik **282**, 170891 (2023a)
Hossain, M., Mondal, K., Kumar, D., Rakshit, J.K., Mandal, S.: Design and study of silicon microring resonator based all-optical binary-coded decimal adder. Opt. Quant. Electron. **55**(12), 1100 (2023b)
https://optics.ansys.com/hc/en-us/articles/360036107074-Eye-Diagram-EYE-NTERCONNECT-Element
Kotiyal, S., Thapliyal, H., Ranganathan, N.: Design of reversible adder-subtractor and its mapping in optical computing domain. In transactions on Computational Science XXIV: Special Issue on Reversible Computing. 37–55 (2014)
Kumar, A., Kumar, M., Jindal, S.K., Raghuwanshi, S.K., Choudhary, R.: Implementation of all-optical 1×4 memory register unit using the micro-ring resonator structures. Opt. Quant. Electron. **53**, 1–35 (2021)
Kundu, S., Hossain, M., Mandal, S.: Modeling of silicon microring resonator-based programmable logic device for various arithmetic and logic operation in Z-domain. Opt. Quant. Electron. **55**(2), 175 (2023)
Landauer, R.: Irreversibility and heat generation in the computing process. IBM J. Res. Dev. **5**(3), 183–191 (1961)
Maji, K., Mukherjee, K., Mandal, M.K.: All optical comparator using tera hertz optical asymmetric demultiplexer (TOAD). J. Nonlinear Optical Phys. Mater. **32**(04), 2350034 (2023)
Mukherjee, K.: Design and analysis of all optical frequency encoded X-OR and X-NOR gate using quantum dot semiconductor optical amplifier-Mach Zehnder Interferometer. Opt. Laser Technol. **140**, 107043 (2021)
Peres, A.: Reversible logic and quantum computers. Phys. Rev. A **32**(6), 3266–3276 (1985)
Qiu, C., Zhang, C., Zeng, H., Guo, T.: High-performance graphene-on-silicon nitride all-optical switch based on a Mach-Zehnder interferometer. J. Lightwave Technol. **39**(7), 2099–2105 (2020)
Raja, A., Mukherjee, K., Roy, J.N.: Design analysis and applications of all-optical multifunctional logic using a semiconductor optical amplifier-based polarization rotation switch. J. Comput. Electron. **20**, 387–396 (2021)
Rakshit, J.K., Hossain, M.: Design and analysis of an efficient reversible hybrid new gate using silicon microring resonator-based all-optical switch. Photon Netw. Commun. **44**(2–3), 116–132 (2022)
Saharia, A., Mudgal, N., Choure, K.K., Maddila, R., Tiwari, M., Singh, G.: Proposed all-optical read-only memory element employing Si3N4 based optical microring resonator. Optik **251**, 168493 (2022)
Sethi, P., Roy, S.: Ultrafast all-optical flip-flops, simultaneous comparator-decoder and reconfigurable logic unit with silicon microring resonator switches. IEEE J. Sel. Top. Quantum Electron. **20**(4), 118–125 (2013)
Sibbett, W., Lagatsky, A.A., Brown, C.T.A.: The development and application of femtosecond laser systems. Opt. Express **20**(7), 6989–7001 (2012)
Singh, M.P., Rakshit, J.K., Hossain, M.: Design of polarization conversion and rotation based ternary logic AND/NAND, OR/NOR, Ex-OR/Ex-NOR gates using ring resonator. Opt. Quant. Electron. **53**(12), 703 (2021)
Song, X., Yang, G., Perkowski, M., Wang, Y.: Algebraic characterization of reversible logic gates. Theory Computing Syst. **39**(2), 311–319 (2006)
Soref, R.: The past, present, and future of silicon photonics. IEEE J. Sel. Top. Quantum Electron. **12**(6), 1678–1687 (2006)
Theresal, T., Sathish, K., Aswinkumar, R.: A new design of optical reversible adder and subtractor using MZI. Int. J. Sci. Res. Publ. **5**(4), 1–6 (2015)
Vardakas, J.S., Zoiros, K.E.: Performance investigation of all-optical clock recovery circuit based on Fabry-Pérot filter and SOA-assisted Sagnac switch. Opt. Eng. **46**(8), 085005 (2007)
Xu, Q., Lipson, M.: All-optical logic based on silicon micro-ring resonators. Opt. Express **15**(3), 924–929 (2007)